INTERNATIONAL JOURNAL FOR NUMERICAL METHODS IN FLUIDS
Int. J. Numer. Meth. Fluids 2009; **61**:709–724
Published online 4 December 2008 in Wiley InterScience (www.interscience.wiley.com). DOI: 10.1002/fld.1971

Permeable and non-reflecting boundary conditions in SPH

Martin Lastiwka, Mihai Basa and Nathan J. Quinlan*, †

Department of Mechanical and Biomedical Engineering, National University of Ireland, Galway, Ireland

SUMMARY

Inflow and outflow boundary conditions are essential for the application of computational fluid dynamics to many engineering scenarios. In this paper we present a new boundary condition implementation that enables the simulation of flow through permeable boundaries in the Lagrangian mesh-free method, smoothed particle hydrodynamics (SPH). Each permeable boundary is associated with an inflow or outflow zone outside the domain, in which particles are created or removed as required. The analytic boundary condition is applied by prescribing the appropriate variables for particles in an inflow or outflow zone, and extrapolating other variables from within the domain. Characteristic-based non-reflecting boundary conditions, described in the literature for mesh-based methods, can be implemented within this framework. Results are presented for simple one-dimensional flows, quasi-one-dimensional compressible nozzle flow, and two-dimensional flow around a cylinder at Reynolds numbers of 40 and 100 and a Mach number of 0.1. These results establish the capability of SPH to model flows through open domains, opening a broad new class of applications. Copyright © 2008 John Wiley & Sons, Ltd.

Received 20 September 2008; Revised 22 October 2008; Accepted 26 October 2008

KEY WORDS: smoothed particle hydrodynamics; boundary conditions; meshfree; particle; Lagrangian; cylinder

1. INTRODUCTION

In many important questions in engineering fluid dynamics, the flow field extends over a very large spatial domain, but the phenomena of interest are restricted to a relatively small region. Examples include turbomachinery, pipes and channels, blood flow and external flows (where the local flow

*Correspondence to: Nathan J. Quinlan, Department of Mechanical and Biomedical Engineering, National University of Ireland, Galway, Ireland.
†E-mail: nathan.quinlan@nuigalway.ie

Contract/grant sponsor: Irish Research Council for Science, Engineering and Technology; contract/grant number: SC/02/189

is governed by conditions in a practically infinite 'free stream'). These problems can be simulated successfully if the computational model is restricted to a small domain of interest, with boundary conditions that provide reasonable models for the interaction of fluid in the domain with fluid in the exterior. In particular, boundary conditions must allow fluid to enter and leave the local computational domain. This approach is well established in Eulerian mesh-based methods.

Mesh-free Lagrangian methods such as smoothed particle hydrodynamics (SPH) have some advantages over conventional methods, particularly in complex flows involving free surfaces and moving bodies. Oger *et al*. [1] and Kajtar and Monaghan [2] give recent examples. However, Lagrangian methods are at a disadvantage in the treatment of permeable boundary conditions. The Eulerian frame of reference naturally describes a stationary spatial region with inflow and outflow of fluid, while the Lagrangian reference frame follows fluid particles that may spend only a short time traversing the spatial region of interest. Flow into and out of a domain can be modelled in SPH with spatial periodicity, but this is accurate only for very special cases, and its use even as an approximation is severely restricted. Furthermore, periodic boundaries cause particle distributions to be recycled through the domain, so that a perturbed particle distribution may degrade without limit over time. While SPH has been successful in the modelling of unbounded (e.g. astrophysical) processes and wall-bounded unsteady flows (e.g. dam-break and wavemaker flows), it has not been widely used for problems with inflow and outflow. To extend the scope of SPH to a wider range of engineering flows, it is essential to incorporate inflow and outflow boundaries.

This paper presents a method for accurate implementation of inflow and outflow boundaries in SPH. The method incorporates a framework for the insertion of new particles at an inflow boundary and the removal of particles at an outflow boundary, while ensuring that appropriate mathematical boundary conditions are enforced. Following some background material in Sections 2 and 3, this framework is described in Section 4, and results are shown for a simple 1D wave propagation problem. In Section 5, a non-reflecting boundary condition due to Giles [3] is described, and its implementation in the new SPH framework is shown. In Section 6, results are presented for the new boundary conditions for compressible flow through a quasi-one-dimensional nozzle and for flow around a cylinder at Reynolds numbers of 40 and 100.

2. SPH DISCRETIZATION

The SPH method has been reviewed in detail by Monaghan [4] and others. SPH is based on gradient approximations of the form

$$\nabla F(\mathbf{x})|_{\mathbf{x}=\mathbf{x}_a} \approx -\sum_b F(\mathbf{x}_b)\nabla W(\mathbf{x}-\mathbf{x}_a, h)|_{\mathbf{x}=\mathbf{x}_b}\frac{m_b}{\rho_b} \tag{1}$$

where $F(\mathbf{x})$ is a field, $\mathbf{x}_a$ is the location of interest, m is particle mass, ρ is density, $W(\mathbf{r}, h)$ is the kernel function and h is the smoothing length. In most implementations, W has compact support and h is defined such that the support radius is kh, where k is a constant. Thus, the summation is a sum over particles b in the neighbourhood of $\mathbf{x}_a$, where $\nabla F(\mathbf{x})$ is to be evaluated. SPH is a mesh-free method because interactions among particles depend only on their locations, and do not require prescribed topological connections.

By applying Equation (1) to the Navier–Stokes equations, the standard SPH formulations given below may be derived [4].

DOI: 10.1002/fld

$$\frac{\mathrm{D}\rho_a}{\mathrm{D}t} = \rho_a \sum_b (\mathbf{u}_a - \mathbf{u}_b) \cdot \nabla W_{ab} \frac{m_b}{\rho_b} \tag{2}$$

$$\frac{\mathrm{D}\mathbf{u}_a}{\mathrm{D}t} = -\sum_b m_b \left(\frac{p_a}{\rho_a^2} + \frac{p_b}{\rho_b^2} + \Pi_{ab} + R_{ab} f_{ab} \right) \nabla W_{ab} \tag{3}$$

$$\frac{\mathrm{D}e_a}{\mathrm{D}t} = \frac{1}{2} \sum_b m_b \left(\frac{p_a}{\rho_a^2} + \frac{p_b}{\rho_b^2} \right) (\mathbf{u}_a - \mathbf{u}_b) \cdot \nabla W_{ab} \tag{4}$$

Here p is pressure, $\mathbf{u}$ is velocity and e is internal energy. For the purposes of the present work, a calorically perfect gas is assumed and the equation of state $p = (\gamma - 1)\rho e$ is used, where γ is the specific heat ratio and e is set to zero at temperature $T = 0$. The notation W_{ab} denotes a kernel function $W(\mathbf{r}, h)$ evaluated with $\mathbf{r} = \mathbf{x}_a - \mathbf{x}_b$. Throughout this paper, the cubic spline kernel of Monaghan and Lattanzio [5] is used for W, with compact support radius $2h$. Because of the symmetry of Equations (2)–(4) with respect to particle indices, and the symmetry of the kernel function (such that $\nabla W_{ab} = -\nabla W_{ba}$), each pairwise particle interaction exactly conserves mass, momentum and energy.

Throughout this work, the basic SPH gradient estimate of Equation (1) is corrected using the mixed gradient and kernel correction method of Bonet and Lok [6]. The basic SPH gradient operation does not exactly reproduce the gradient of a constant-valued function (i.e. it is not zero-order consistent). Bonet and Lok have shown that their corrected gradient applied to a Shepard-corrected kernel ensures first-order consistency and exact conservation of linear and angular momentum (although it results in a loss of exact energy conservation). Consistency correction gives a marked improvement in accuracy where the particle distribution is non-uniform or the particle support is incomplete (i.e. the number of neighbour particles is low) [7]. This is the main motivation for use of a correction in the present work, since incomplete support is unavoidable in SPH operations near boundaries.

In the momentum equation, Π_{ab} is the viscous stress between particles a and b. For one-dimensional and quasi-one-dimensional flow in the present work, we use the following artificial viscosity formulation introduced by Monaghan and Gingold [8] to enable shock capturing:

$$\Pi_{ab} = \begin{cases} (-\alpha c_{ab} \varphi_{ab} + \beta \varphi_{ab}^2)/\rho_{ab} & \text{if } \mathbf{u}_{ab} \cdot \mathbf{r}_{ab} < 0 \\ 0 & \text{otherwise} \end{cases} \tag{5}$$

where φ_{ab} is defined by

$$\varphi_{ab} = \frac{h \mathbf{u}_{ab} \cdot \mathbf{r}_{ab}}{r_{ab}^2 + \eta^2} \tag{6}$$

In the above, c_{ab} and ρ_{ab} are averages over particles a and b of the speed of sound and density, respectively, $\mathbf{r}_{ab} = \mathbf{r}_b - \mathbf{r}_a$ and $\mathbf{u}_{ab} = \mathbf{u}_b - \mathbf{u}_a$. The constant coefficients α and β determine the strength of the dissipation and the term η, defined as $h/10$, serves to prevent a singularity when $\mathbf{r}_{ab} = 0$. For two-dimensional viscous flow applications, the viscous stress is approximated by the following SPH/finite-difference combination, following Violeau and Issa [9]:

$$\Pi_{ab} = \frac{-8}{\rho_a + \rho_b} \mu \left(\frac{1}{\rho_a} + \frac{1}{\rho_b} \right) \frac{\mathbf{u}_{ab} \cdot \mathbf{r}_{ab}}{r_{ab}^2 + \eta^2} \tag{7}$$

DOI: 10.1002/fld

where μ is the physical viscosity coefficient. Particles a and b exchange equal and opposite viscous interparticle forces directed parallel to the displacement between the particles. Therefore, this formulation conserves linear and angular momentum. These properties are discussed more fully by Violeau and Issa [9] and Basa *et al*. [10].

The term $R_{ab} f_{ab} \nabla W_{ab}$ is Monaghan's interparticle force [11] defined by

$$f_{ab} = \frac{W(r_{ab}, h)}{W(\overline{r}_{ab}, h)} \tag{8}$$

and

$$R_{ab} = \zeta \left(\frac{p_a}{\rho_a^2} + \frac{p_b}{\rho_b^2} \right) \tag{9}$$

where $\overline{r}_{ab}$ is the local average interparticle spacing and ζ is a constant. This term acts as a small short-range interparticle repulsive force and was introduced to suppress the tensile instability in some applications. Since the ideal gas equation of state is used in the present work, pressure is always positive and the tensile instability does not arise, according to the analysis of Swegle *et al*. [12]. However, in application to separated flow (Section 6.2) particle voids may occur in the wake of a bluff body, and we have found that the inclusion of $R_{ab} f_{ab}$ in the momentum equation is effective in maintaining an adequate particle distribution.

3. CHARACTERISTIC THEORY FOR BOUNDARY CONDITIONS

The method of characteristics provides a rigorous analytical framework for the implementation of boundary conditions in numerical methods [13, 14]. If the flow is normal to the boundary and free of shock waves and significant viscous effects, it is governed by the one-dimensional Euler equations for isentropic flow of a calorically perfect gas. (In practice, these conditions can often be satisfied or approximated by suitable placement of the permeable computational boundaries.) It can then be shown that three characteristic variables or Riemann invariants (J_+, J_- and entropy s) exist, which are constant along curves in the x–t (space–time) plane defined by $\mathrm{d}x/\mathrm{d}t = u+a, u-a, u$ respectively, where a is the speed of sound. These curves can be interpreted as the trajectories of sound waves and material particles that carry constant values of the characteristic variables. The characteristic variables J_+ and J_- are given by $J_\pm = u \pm 2a/(\gamma - 1)$.

This approach guides the numerical implementation of boundary conditions because it frames the governing equations in terms of information propagation. For subsonic flow ($u < a$), there are always two characteristic waves running downstream at velocities u and $u+a$, with one characteristic carrying information upstream at $u-a$. Where flow enters the domain through an inflow boundary, therefore, we should prescribe the downstream-running characteristics J_+ and s (based on knowledge of conditions outside the domain) and determine J_- from the solution inside the domain (in other words, allow the value of J_- to propagate upstream to the boundary). Similarly, at an outflow boundary, the method of characteristics suggests that J_- should be prescribed (i.e. determined from the exterior of the domain), while J_+ and s should be transmitted from the domain interior. (A similar analysis can be made for supersonic flow.)

In practice, however, it is difficult to implement characteristic-based boundary conditions rigorously because J_+, J_- and s are rarely known, and their value outside the domain may not be

DOI: 10.1002/fld

independent of events inside the domain. Variables such as velocity, pressure and temperature, on the other hand, often are known or can be measured for the physical flow that is to be modelled. At a minimum, however, the method of characteristics determines the number of variables that should be prescribed at the boundary (to propagate into the domain) and the number which should be propagated from the domain interior to the boundary.

4. TREATMENT OF LAGRANGIAN PARTICLES AT EULERIAN BOUNDARIES

Since Lagrangian SPH particles are not constrained to the boundaries of an Eulerian (i.e. spatially fixed) domain, new particles must be defined at inlets and removed at outlets, at a rate consistent with the physical flow rate across each boundary. In this section, an algorithmic framework is presented for this process. A schematic diagram of the implementation for inflow boundaries is shown in Figure 1. The method as presented here requires that the boundary is planar and that flow is normal to the boundary (in practice this can be achieved by placing the inlet boundary far enough upstream of any flow features that may cause the flow to be non-unidirectional). The inflow velocity may vary in time and/or space. It is also required that a compactly supported kernel function is used in the underlying SPH method.

An inflow zone is defined outside the flow domain by extruding the inlet boundary in the upstream direction. The length of the inflow zone in the flow direction is equal to or greater than the support radius of the SPH kernel function. Every time a particle crosses from the inflow zone to the fluid domain, a new particle is created at the upstream side of the inflow zone. This approach maintains the required particle number density at the inflow boundary.

The updating of particle variables inside the inflow zone depends on the analytical boundary condition to be applied. For subsonic flow, the method of characteristics suggests that two variables must be prescribed while one is determined from the domain interior. An intuitive choice is to prescribe velocity and temperature at the inflow boundary, leaving pressure or density to be

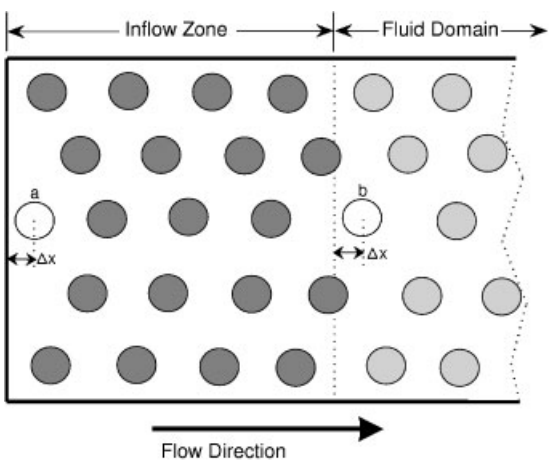

Figure 1. Schematic diagram of the inflow boundary zone. A new particle *a* is added when an existing particle *b* crosses out of the inlet zone into the fluid domain.

DOI: 10.1002/fld

determined by information propagating upstream from the interior. (Prescription of temperature is equivalent to prescription of internal energy in the present work, since a calorically perfect gas is modelled.) To implement this boundary condition within this SPH framework, the velocity and temperature are prescribed for every particle in the inflow zone. Pressure at inflow particles is then determined by an SPH interpolation based only on information from neighbour particles that are inside the domain. This amounts to an extrapolation from the interior domain into the boundary zone. Since this extrapolation is carried out with incomplete and one-sided support, a standard SPH interpolation would yield very poor results. For this purpose we use the reproducing kernel particle method of Liu *et al*. [15], which gives first-order consistency in the boundary extrapolations.

Particles near the boundary, but inside the fluid domain, are updated according to usual SPH procedures. Some inflow zone particles fall inside the compact support of near-boundary fluid particles, and thus allow boundary information to be propagated into the domain.

The outflow zone, defined downstream of the fluid domain, is simpler to implement since no new particles need to be created. In this zone, one variable is prescribed to represent the downstream conditions. If velocity and temperature are prescribed at the inlet, as described above, then pressure or density can be prescribed at the outlet. Extrapolation of the other two variables to the outlet is effectively performed by convection of particles from the domain interior to the outflow zone. The governing equations are still solved for these outflowing particles until they flow past the downstream limit of the outlet zone and are eliminated from the simulation. Again, because SPH

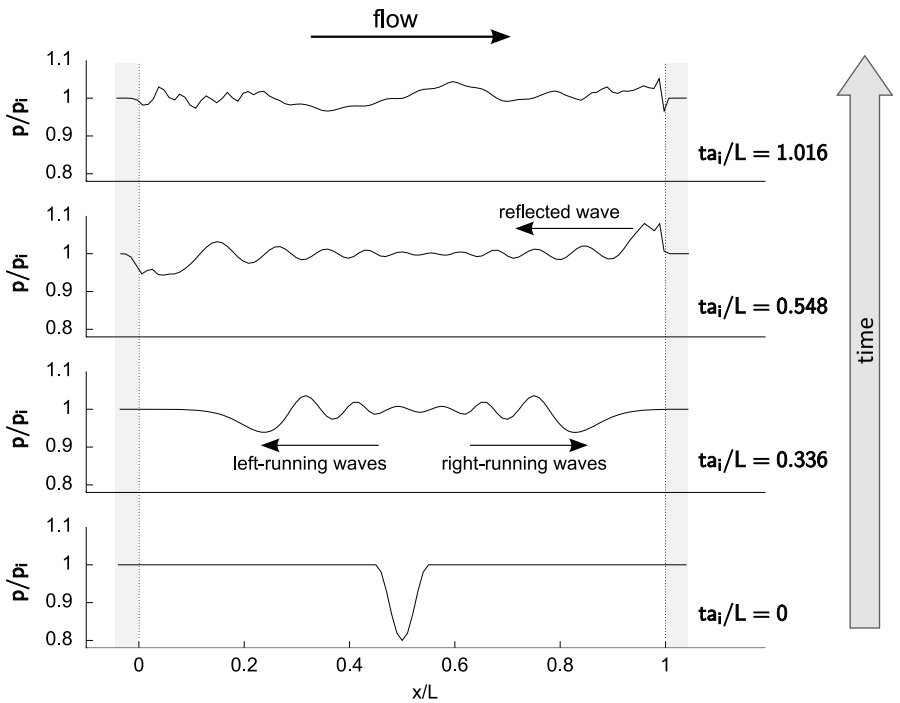

Figure 2. Pressure distribution at various times in a simulation of an one-dimensional flow at $M=0.1$ with an initial perturbation in the pressure field. Velocity and temperature are prescribed at the inlet, $x=0$, and pressure is prescribed at the outlet, $x=L$. Shaded bands denote the inflow and outflow zones.

DOI: 10.1002/fld

operations are performed on the outflow particles with incomplete support, at least zero-order consistency is required.

These boundary conditions were tested for a simulation of one-dimensional compressible flow of an ideal gas in the domain $0 \leqslant x \leqslant L$. Particles are distributed at an initial spacing of $\Delta x_i / L = 0.01$, with $h/\Delta x_i = 1.7$. Artificial viscosity is used with $\alpha = 0.1$ and $\beta = 0$ in Equation (5), and the artificial repulsive force of Equation (8) is not used. Uniform pressure, velocity and temperature are set as p_i, u_i and T_i, respectively, in the initial condition. The initial Mach number $M_i = u_i / \sqrt{\gamma R T_i}$ is 0.1. At the inlet ($x = 0$) velocity and temperature are prescribed as u_i and T_i using the method described above, and at the outlet ($x = L$) the pressure is prescribed as p_i. For this trivial problem, the steady-state solution is equal to the initial conditions, and SPH successfully maintains the solution. However, if the initial condition is perturbed by introducing a region where $p(x) < p_i$, left- and right-running waves are expected. These waves must be transmitted out of the domain before the uniform steady state can be reached. This is a more challenging test of the boundary condition algorithm, and results are presented in Figure 2 for an initial perturbation equal to 20% of the absolute background pressure p_i. In the results, time is normalized with respect to L/a_i, the time required for a sound wave to traverse the domain at the initial speed of sound, a_i.

The results show that the algorithm successfully enforces the prescribed inlet and outlet conditions. However, waves arriving at the boundaries around $t a_i / L = 0.5$ are reflected back into the domain, and they delay convergence towards steady state. This is non-physical behaviour, since waves should propagate freely through the boundaries just as they propagate through the interior domain. In the example shown, the computation fails shortly after $t a_i / L = 1.016$, with the development of large particle voids near a boundary. However, the significance of this result is that SPH can indeed simulate permeable boundaries defined at fixed Eulerian locations using the framework of inflow and outflow zones described above. The accuracy and robustness of the method can be improved by a more appropriate choice of analytical boundary condition, as shown in the next section.

5. NON-REFLECTING BOUNDARY CONDITIONS

The problem of undesirable wave reflection at boundaries is well known. In principle, it can be removed by a characteristic formulation of the boundary conditions, as discussed in Section 3. However, it is difficult in practice to determine the appropriate boundary values of the exact characteristics of the Euler equations. Giles [3] proposed alternative boundary conditions based on a linearized set of governing equations, assuming that perturbations from a uniform, steady reference flow are small near the boundaries. Giles derived the following set of characteristic variables for the linearized equations:

$$J_1 = -a^2(\rho - \rho_{\text{ref}}) + (p - p_{\text{ref}}) \tag{10}$$

$$J_2 = \rho a(u - u_{\text{ref}}) + (p - p_{\text{ref}}) \tag{11}$$

$$J_3 = -\rho a(u - u_{\text{ref}}) + (p - p_{\text{ref}}) \tag{12}$$

The subscript ref denotes the reference flow near the boundaries, which can be prescribed on the basis of knowledge of the exterior domain. The first characteristic wave is associated with convection of entropy and propagates at flow velocity. The second and third characteristics are

DOI: 10.1002/fld

waves that propagate upstream and downstream relative to the local flow. At an inflow boundary, the downstream-running characteristics J_1 and J_2 should be prescribed as zero and the upstream-running characteristic J_3 should be determined from the domain interior. Similarly, at the outflow boundary, J_1 and J_2 should be determined from the interior, while the boundary condition is $J_3 = 0$. By inverting the system of equations (10)–(12), it is straightforward to express pressure, density and velocity as functions of the characteristic variables, as shown below.

$$\rho - \rho_{\text{ref}} = \frac{1}{a^2}\left(-J_1 + \frac{1}{2}J_2 + \frac{1}{2}J_3\right) \tag{13}$$

$$u - u_{\text{ref}} = \frac{1}{2\rho a}(J_2 - J_3) \tag{14}$$

$$p - p_{\text{ref}} = \tfrac{1}{2}(J_2 + J_3) \tag{15}$$

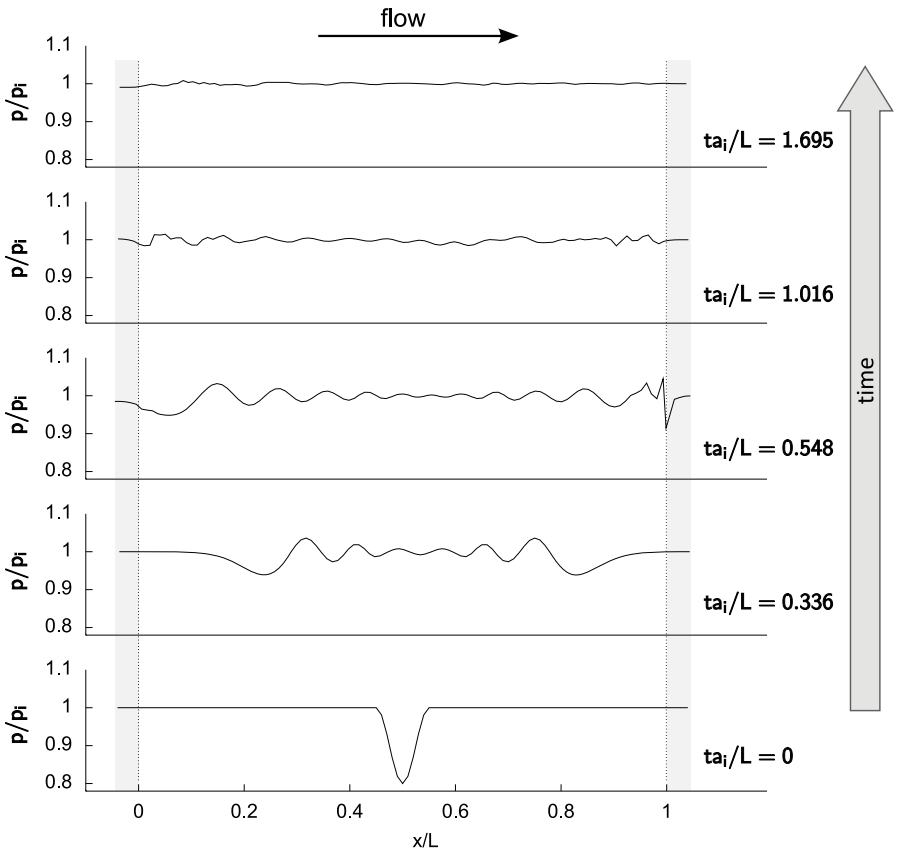

Figure 3. Pressure distribution at various times in a simulation of an one-dimensional flow at $M = 0.1$, with an initial perturbation in the pressure field. Non-reflecting inlet and outlet boundary conditions are applied. Shaded bands denote the inflow and outflow zones.

DOI: 10.1002/fld

These equations are used to update ρ, u and p at the boundaries after the characteristics have been determined. The reference values (about which the governing equations are linearized) must be specified for all three variables at both boundaries. This is not equivalent to prescription of ρ, u and p, since perturbations from the reference flow are allowed. The boundary conditions are imposed on J_1, J_2 and J_3 rather than ρ, u and p. The implementation of this analytical boundary condition in SPH is straightforward within the framework described in Section 4.

The one-dimensional steady-flow test case was repeated with these non-reflecting boundary conditions. Results are shown in Figure 3. Waves are attenuated significantly on reflection, in comparison with the case shown in Figure 2. By dimensionless time $ta_i/L=1.695$, perturbation from the steady state has decayed to less than 5% of its original value because waves have been transmitted out through the boundaries.

6. APPLICATIONS

In this section, results are reported for flow simulations that make use of the inflow and outflow boundary implementations. A quasi-one-dimensional nozzle simulation is used to demonstrate subsonic and supersonic inflow and outflow. This is followed by simulations of steady and unsteady two-dimensional flow around a cylinder.

6.1. Quasi-one-dimensional nozzle flow

In these test cases, an inviscid ideal gas flows through a duct of non-uniform cross-sectional area, and all variables are assumed to be functions of x only, with negligible y and z velocity components. Flow is governed by the quasi-one-dimensional Euler equations

$$\frac{\partial}{\partial t}\begin{pmatrix}\rho A\\ \rho u A\\ \rho\left(e+\frac{1}{2}u^2\right)A\end{pmatrix}+\frac{\partial}{\partial x}\begin{pmatrix}\rho u A\\ \rho u^2 A\\ \rho u\left(e+\frac{1}{2}u^2+p/\rho\right)A\end{pmatrix}+A\frac{\partial}{\partial x}\begin{pmatrix}0\\ p\\ 0\end{pmatrix}=0 \tag{16}$$

where $A=A(x)$ is the cross-sectional area of the duct. These equations can be discretized using standard SPH methods. For steady isentropic flow, an exact solution is given by

$$\left(\frac{A}{A^*}\right)^2=\frac{1}{M^2}\left[\frac{2}{\gamma+1}\left(1+\frac{\gamma-1}{2}M^2\right)\right]^{\gamma+1/\gamma-1} \tag{17}$$

where M is the Mach number and A^* is the critical area (at which $M=1$) [16].

The duct is a convergent–divergent nozzle with inlet area 2 (arbitrary units), throat area 1 and outlet area 1.3. In this geometry, the outlet and inlet areas are different and the outlet and inlet flow conditions are different. This entirely precludes the use of periodic boundaries, even as an approximation to inflow and outflow boundaries. Inflow and outflow zones are used, as described in Section 4. In the initial conditions, particles are distributed uniformly over the length L of the domain at an initial spacing $\Delta x_i/L=0.01$, with smoothing length $h=4/3\Delta x_i$. Artificial viscosity is used with $\alpha=1.5$ and $\beta=2.5$, and there is no artificial repulsive force.

For the inlet with subsonic flow, total pressure p_0 and total temperature T_0 are prescribed for all particles in the inflow zone, while static pressure p is extrapolated from the domain interior. At

DOI: 10.1002/fld

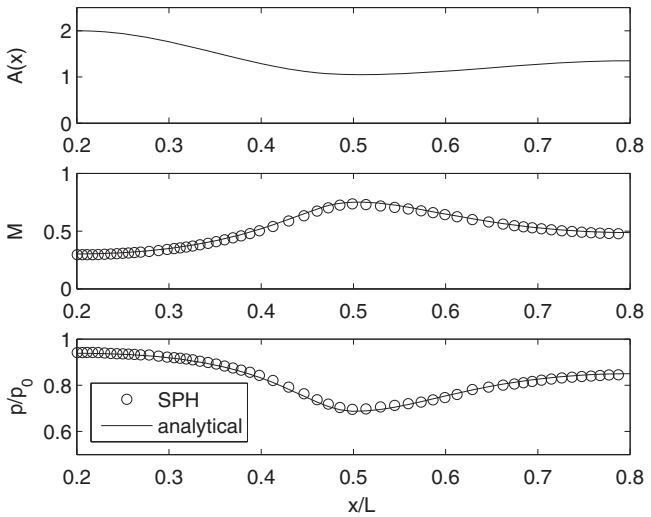

Figure 4. Area, Mach number and pressure ratio distributions in the quasi-one-dimensional nozzle with subsonic inlet and subsonic outlet, computed with SPH and from an exact analytical solution.

the outlet, for subsonic flow, static pressure is prescribed while energy and velocity are determined from the conservation equations. Final steady-state results for this case are shown in Figure 4. The SPH solution is in excellent agreement with the analytical solution, with root mean square error less than 1% in pressure and Mach number.

In supersonic flow, no characteristics propagate upstream. Thus, at a supersonic inlet, three variables must be prescribed (total pressure p_0, total temperature T_0 and static pressure p in this case). At a supersonic outlet, all variables are determined in the outflow zone by solution of the discrete conservation equations, with the neighbour deficiency for the most downstream particles effectively enforcing one-way propagation of information. Results are shown in Figure 5 for a nozzle flow with entirely supersonic flow from inlet to outlet. (This is a purely theoretical scenario, since the decelerating flow would contain oblique shocks in a physical nozzle. It is the quasi-one-dimensional analytical model, rather than the numerical approximation, which fails to capture the physics completely.) Again, there is very good agreement with the analytical result. Root mean square errors are 3.2% and 0.8% for Mach number and pressure, respectively. These simple but non-trivial test cases provide an effective preliminary validation of the new approach to modelling inflow and outflow boundaries in SPH.

6.2. *Two-dimensional flow over a cylinder at* $Re_D = 40$

Two-dimensional flow over a cylinder is a classic fluid dynamics study, and an important test for numerical methods. Lee *et al*. [17] simulated flow over a square cylinder using SPH, with periodic boundaries upstream and downstream and a streamwise body force to overcome drag. This arrangement represents the special case of a cylinder in an infinite array. Takeda *et al*. [18] used SPH to model flow over a cylinder at Reynolds numbers from 6 to 55, but performed a separate finite-difference simulation to provide boundary conditions for SPH. For a general model of flow over a cylinder or any body immersed in a steady flow, true inflow and outflow boundaries are required. To date there has been no complete SPH simulation of this case.

DOI: 10.1002/fld

The geometric definition of this problem is shown in Figure 6. Flow is from left to right as shown in the diagram, with periodic boundaries used at the top and bottom. The solid cylinder is modelled using fixed particles placed in concentric circles. Approximately 10 000 fluid particles are used in the simulation, initially distributed in concentric circles near the cylinder and on a Cartesian grid further away. The initial particle spacing Δx is approximately $(0.11)D$ and the smoothing length is $h=(0.22)D$, where D is the cylinder diameter. The Mach number (based on inlet reference velocity and temperature) is 0.1. The fluid is modelled using the mixed gradient and kernel correction of Bonet and Lok [6] for first-order consistency, and Monaghan's repulsive force term defined in Equation (8) [11] with $\zeta=0.05$ to suppress particle voids. Viscous stresses are modelled using Equation (7).

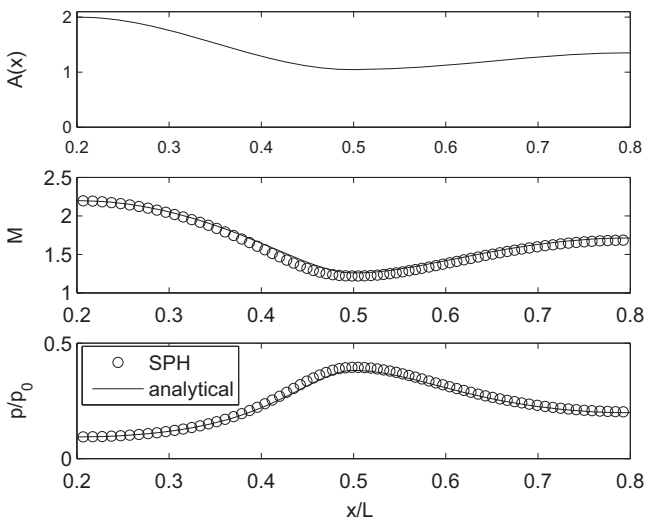

Figure 5. Area, Mach number and pressure ratio distributions in the quasi-one-dimensional nozzle with supersonic inlet and supersonic outlet, computed with SPH and from an exact analytical solution.

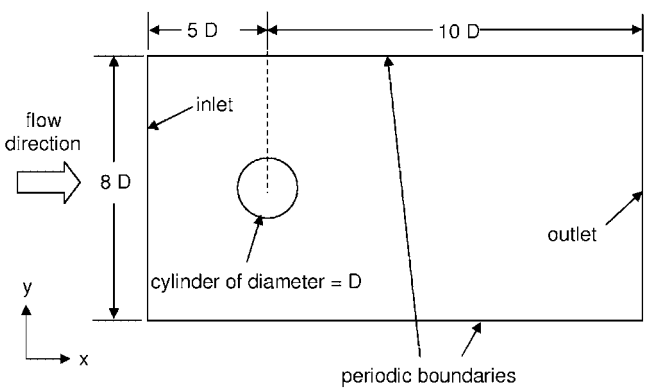

Figure 6. Domain geometry for the model of two-dimensional flow around a cylinder.

DOI: 10.1002/fld

Two simulations were carried out for a Reynolds number Re_D of 40 (based on cylinder diameter and inlet velocity). At this value of Re_D, flow is expected to be laminar everywhere, with a pair of steady, symmetric counter-rotating vortices in the wake. Unsteady vortex shedding occurs at Reynolds numbers above about 45 [19]. In the first simulation, velocity and temperature were simply prescribed at the inlet, and pressure was prescribed at the outlet. In the second, the non-reflecting boundary conditions of Giles were applied at the inlet and outlet. In both cases, the boundary conditions were imposed within the framework of inflow and outflow zones as described in Section 4. Results for dimensionless pressure coefficient $c_p = (p(\theta) - p_\infty)/\frac{1}{2}\rho_\infty u_\infty^2$ over the cylinder are shown in Figures 7 and 8 for the prescribed and non-reflecting boundary conditions, respectively (where θ is the polar angle about the centre of the cylinder). (The freestream conditions p_∞, ρ_∞ and u_∞ are taken as the inlet conditions for the purpose of computing c_p.) Results shown include time averages over 4000 steps (excluding a start-up period), with error bars indicating the root-mean-square deviation over this period. Also shown are time averages over typical periods of 50 time steps. For the case with non-reflecting boundary conditions, the pressure distribution is in reasonable agreement with a prediction from the commercial finite volume software ANSYS-CFX [20], although there is a marked discrepancy in the region of separated flow. Unsteadiness is greatly reduced by the introduction of non-reflecting boundary conditions. The magnitude of fluctuations in surface pressure (indicated by error bars) is reduced by a factor ranging from 1.7 to 8. The greater unsteadiness in the case with prescribed velocity, temperature and pressure boundary conditions is due to waves that traverse the domain and are reflected at the inlet and outlet boundaries. These waves occur in both simulations, but are heavily attenuated by the non-reflecting boundary conditions.

Contour plots of velocity magnitude near the cylinder are shown in Figure 9 for the finite volume and SPH simulations, respectively. Both results predict a steady, symmetric flow separation, and the velocity distributions are in good agreement.

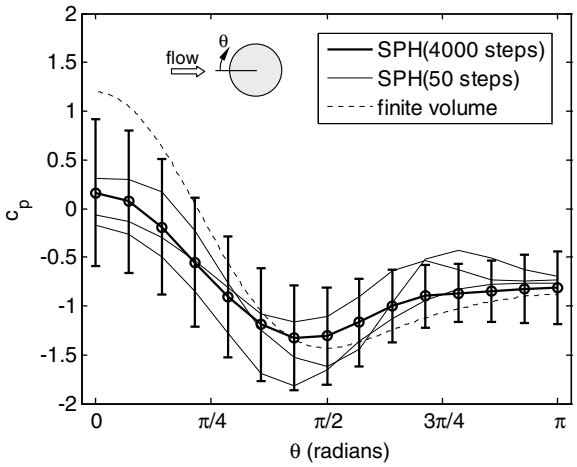

Figure 7. Pressure coefficient on the cylinder surface at $Re_D = 40$, computed using SPH with prescribed velocity, temperature and pressure boundary conditions. Results show time averages over 4000 time steps and over various representative 50 step periods. Error bars show root-mean-square deviation about the 4000 step average. A finite volume solution is shown for comparison.

DOI: 10.1002/fld

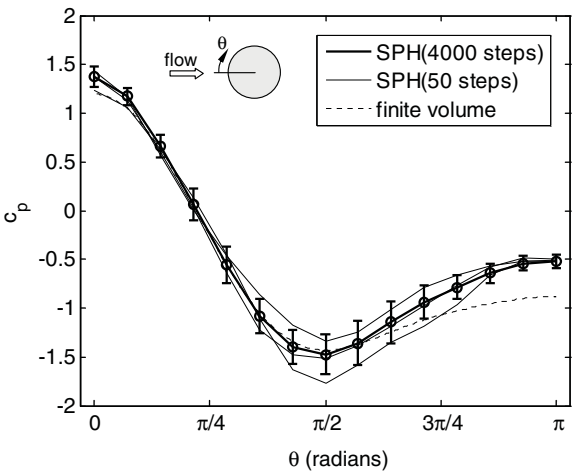

Figure 8. Pressure coefficient on the cylinder surface at $Re_D = 40$, computed using SPH with non-reflecting boundary conditions. Results show time averages over 4000 time steps and over various representative 50 step periods. Error bars show root-mean-square deviation about the 4000 step average. A finite volume solution is shown for comparison.

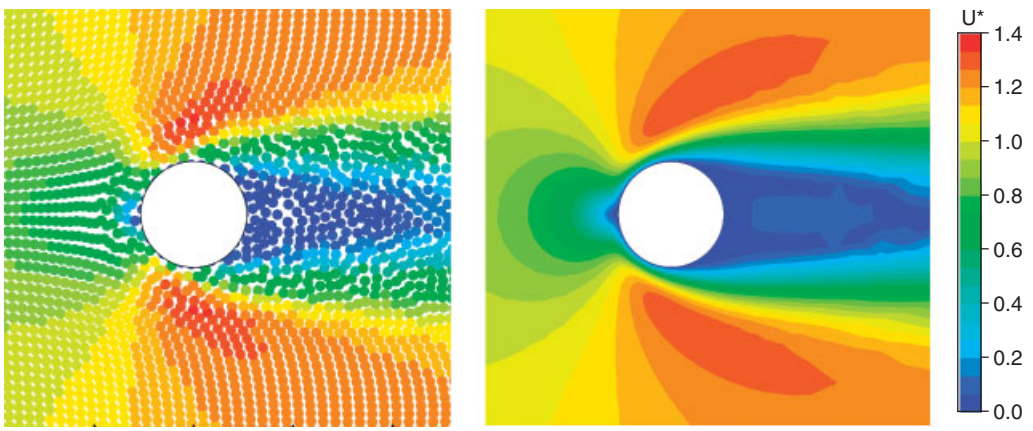

Figure 9. Contour plots of speed, normalized to inlet velocity, in flow around a cylinder at $Re_D = 40$ from (a) an SPH solution with non-reflecting boundary conditions and (b) a finite volume solution.

6.3. Two-dimensional flow over a cylinder at $Re_D = 100$

Flow over a cylinder at a higher Reynolds number of 100 was simulated using the same SPH methods described above with non-reflecting boundary conditions only. At this Reynolds number, an unsteady von Kármán street is expected in the cylinder wake.

A particle spacing and smoothing length of approximately half the values used for $Re_D = 40$ were found necessary in this case because of the thinner boundary and shear layers. Since this higher

DOI: 10.1002/fld

resolution is required only near the cylinder and centreline of the domain, particles were distributed non-uniformly in the transverse (y) direction. The use of a first-order consistency-corrected SPH formulation makes this possible, significantly reducing the error due to particle non-uniformity [7]. The inflow boundary formulation used here automatically preserves the non-uniform particle distribution through the run, since particles are introduced in the inflow zone at the same transverse location where they cross into the interior domain. The non-uniform particle distribution reduced the computational cost by a factor of about 3 relative to a uniform distribution.

The SPH simulation correctly predicts the existence of vortex shedding at this Reynolds number, as shown in Figure 10. The non-uniform distribution of particles is also visible in these visualizations. The SPH simulation predicts a Strouhal number of 0.18, which is in reasonable agreement with the value of 0.165 measured consistently in various experiments [21]. It should be noted that the simulated channel is narrow in comparison with classical studies of cylinder flow, with width equal to 8 cylinder diameters, and this may have some influence on the results.

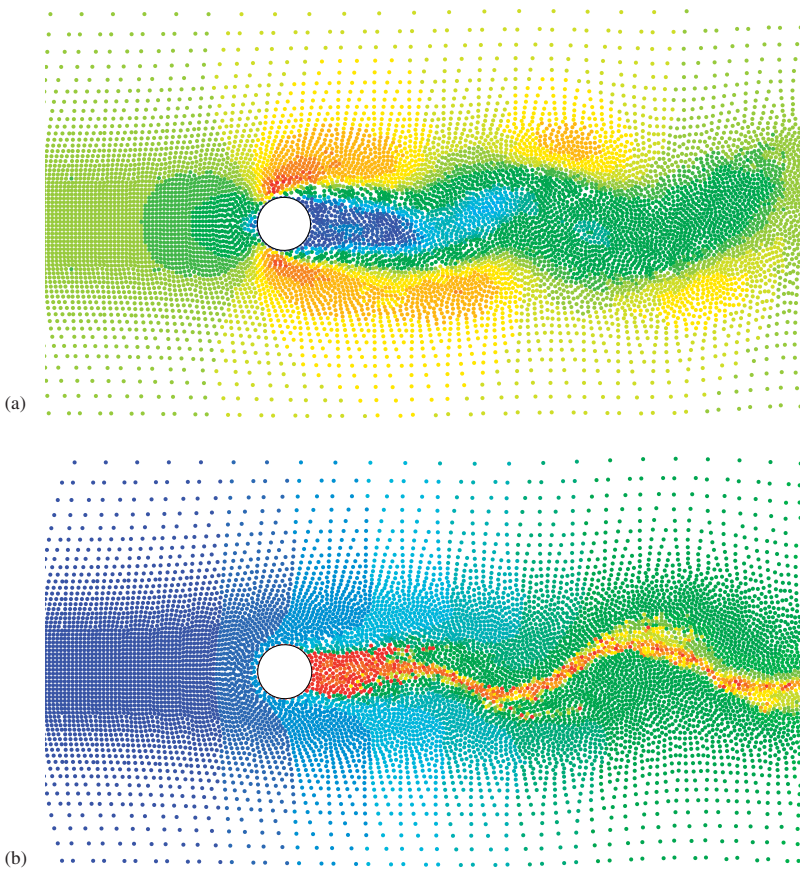

Figure 10. Flow around a cylinder at $Re_D = 100$, from an SPH solution with non-reflecting boundary conditions. (a) Instantaneous contour plot of speed and (b) Instantaneous contour plot of x material (Lagrangian) coordinates. Particles with similar shading had similar x coordinates at the beginning of the simulation.

DOI: 10.1002/fld

7. DISCUSSION

In this paper, a novel framework has been presented for modelling inlet and outlet boundaries in SPH. The method involves inflow and outflow zones outside the flow domain, in which appropriate parameters are prescribed and the SPH equations are partially solved. This framework is flexible enough to allow various analytical forms of inlet or outlet boundary condition to be imposed. In particular, characteristic-based non-reflecting boundary conditions may be applied. Accurate results have been obtained for one-dimensional and quasi-one-dimensional test cases. In two dimensions, the inlet and outlet boundary conditions were used to model flow over a cylinder at Reynolds numbers of 40 and 100, as a classic case of steady-flow rate through a fixed spatial domain. Reasonably accurate results were obtained for pressure distribution, velocity fields and vortex shedding frequency. Qualitative differences between the wake structures at two Reynolds numbers were predicted correctly. The higher Reynolds number case also demonstrated the capability of the method to deal with non-uniform particle distributions and an unsteady, non-uniform outlet condition. These are the first complete SPH simulations of flow over a cylinder achieved without the assumption of streamwise periodicity. The results demonstrate the method's capability to model steady and quasi-steady non-enclosed flows, including separated flow.

In principle, these boundary conditions may be extended to curved boundaries, non-uniform boundary conditions (e.g. a prescribed velocity profile), unsteady boundary conditions and fully incompressible flow. The only restriction is that the flow near the boundary should be uni-directional, so that the one-dimensional approximation remains valid for flow along streamlines. A non-reflecting formulation would not be necessary or applicable for fully incompressible flow, since information is not propagated by acoustic waves. However, further invesitgation is required. Implementation for free-surface flow (an important application area of SPH) is less obvious, since the water depth at outflow must be prescribed. Another possible application of the technique is to the coupling of SPH to a mesh-based method. With boundary conditions of the type presented here, fully Lagrangian modelling of flow through fixed domains is possible, and the scope of SPH is extended to a much broader range of engineering fluid dynamics applications.

ACKNOWLEDGEMENTS

This work was supported by the Irish Research Council for Science, Engineering and Technology, funded by the National Development Plan.

REFERENCES

1. Oger G, Doring M, Alessandrini B, Ferrant P. Two-dimensional SPH simulations of wedge water entries. *Journal of Computational Physics* 2006; **213**(2):803–822.
2. Kajtar J, Monaghan JJ. SPH simulations of swimming linked bodies. *Journal of Computational Physics* 2008; **227**(19):8568–8587.
3. Giles M. Non-reflecting boundary conditions for Euler equations. *AIAA Journal* 1990; **28**(12):2050–2058.
4. Monaghan JJ. Smoothed particle hydrodynamics. *Reports on Progress in Physics* 2005; **68**:1703–1759.
5. Monaghan JJ, Lattanzio JC. Further studies of a fragmentation problem. *Astronomy and Astrophysics* 1986; **158**(1–2):207–211.
6. Bonet J, Lok TSL. Variational and momentum preservation aspects of smooth particle hydrodynamic formulations. *Computer Methods in Applied Mechanics and Engineering* 1999; **180**(1–2):97–115.
7. Quinlan NJ, Lastiwka M, Basa M. Truncation error in mesh-free particle methods. *International Journal for Numerical Methods in Engineering* 2006; **66**(13):2064–2085.

DOI: 10.1002/fld

8. Monaghan JJ, Gingold RA. Shock simulation by the particle method SPH. *Journal of Computational Physics* 1983; **52**(2):374–389.
9. Violea D, Issa R. Numerical modelling of complex turbulent free-surface flows with the SPH method: an overview. *International Journal for Numerical Methods in Fluids* 2007; **53**:277–304.
10. Basa M, Lastiwka M, Quinlan NJ. Robustness and accuracy of SPH formulations for viscous flow. *International Journal for Numerical Methods in Fluids* 2008; DOI: 10.1002/fld.1927.
11. Monaghan JJ. SPH without a tensile instability. *Journal of Computational Physics* 2000; **159**(2):290–311.
12. Swegle JW, Hicks DL, Attaway SW. Smoothed particle hydrodynamics stability analysis. *Journal of Computational Physics* 1995; **116**:123–134.
13. Moretti G. Importance of boundary conditions in the numerical treatment of hyperbolic equations. *Physics of Fluids* 1969; **12**(12):13–20.
14. Hirsch C. *Numerical Computation of Internal and External Flows*, *Volume 2*: *Computational Methods for Inviscid and Viscous Flows*. Wiley: Chichester, 1990.
15. Liu WK, Jun S, Li S, Adee J, Belytschko T. Reproducing kernel particle methods for structural dynamics. *International Journal for Numerical Methods in Engineering* 1995; **38**(10):1655–1679.
16. Shapiro AH. *Dynamics and Thermodynamics of Compressible Flow*. Ronald Press: New York, 1953.
17. Lee ES, Moulinec C, Xu R, Violeau D, Laurence D, Stansby P. Comparisons of weakly compressible and truly incompressible algorithms for the SPH mesh free particle method. *Journal of Computational Physics* 2008; **227**(18):8417–8536.
18. Takeda H, Miyama SM, Sekiya M. Numerical simulation of viscous flow by smoothed particle hydrodynamics. *Progress of Theoretical Physics* 1994; **92**(5):939–960.
19. Jackson DP. A finite-element study of the onset of vortex shedding in flow past variously shaped bodies. *Journal of Fluid Mechanics* 1987; **182**:23–45.
20. Jackson DP. *ANSYS-CFX Reference Guide*. Ansys, Inc.: Canonsburg, 2006.
21. Williamson CHK. Vortex dynamics in the cylinder wake. *Annual Review of Fluid Mechanics* 1996; **28**:477–539.